

Evolution of X-ray Cavities in Galaxy Clusters

Marcus Brüggen*, Evan Scannapieco[†] and Sebastian Heinz**

**Jacobs University Bremen, Campus Ring 1, 28759 Bremen, Germany*

†School of Earth and Space Exploration, Arizona State University, P.O. Box 871404, Tempe, AZ, 85287-1404, USA

***Department of Astronomy, University of Wisconsin, 475 N Charter Street Madison, WI 53706, USA*

Abstract.

The physics of X-ray cavities in galaxy clusters can be constrained by their observed morphological evolution, which is dependent on such poorly-understood properties as the turbulent density field and magnetic fields. Here we combine numerical simulations that include subgrid turbulence and software that produces synthetic X-ray observations to examine the evolution of X-ray cavities in the absence of magnetic fields. Our results reveal an anisotropic size evolution that is very different from simplified, analytical predictions. These differences highlight some of the key issues that must be accurately quantified when studying AGN-driven cavities, and help to explain why the inferred pV energy in these regions appears to be correlated with their distance from the cluster center. Interpreting X-ray observations will require detailed modeling of effects including mass-entrainment, distortion by drag forces, and projection. Current limitations do not allow a discrimination between purely hydrodynamic and magnetically-dominated models for X-ray cavities.

Keywords: galaxy clusters, hydrodynamics

PACS: 98.65.-r, 98.65.Cw, 98.65.Hb

INTRODUCTION

The nature of AGN-driven X-ray cavities remains one of the major outstanding questions in understanding the physics of cool-core galaxy clusters. While the observed morphologies and sizes of the cavities provide us with useful clues as to the processes at work in these regions, interpretation of the observations is far from straightforward. Notably, it is unclear how far AGN-driven cavities rise in the cluster, how they couple to the surrounding medium, and how they evolve.

More specifically, the presence of these cavities has raised a number of key questions. The buoyant bubbles inflated by the central AGN are unstable to the Rayleigh-Taylor (RT) instability, which occurs whenever a fluid is accelerated or supported against gravity by a fluid of lower density. Yet, these cavities appear to be intact even after inferred ages of several 10^8 yrs, as is the case for the outer cavities in Perseus [1]. On the other hand, purely hydrodynamic simulations fail to reproduce these observations. Instead, the RT and other instabilities shred the bubbles in a relatively short time [2, 3]. The time scales of the RT in bubbles are calculated in [4]. Magnetic fields have been shown to alleviate this problem somewhat [5, 6, 7], but they also reduce the extent to which the interior of the hot bubbles couples to the surrounding medium, making it much more difficult for AGN heating to balance cooling.

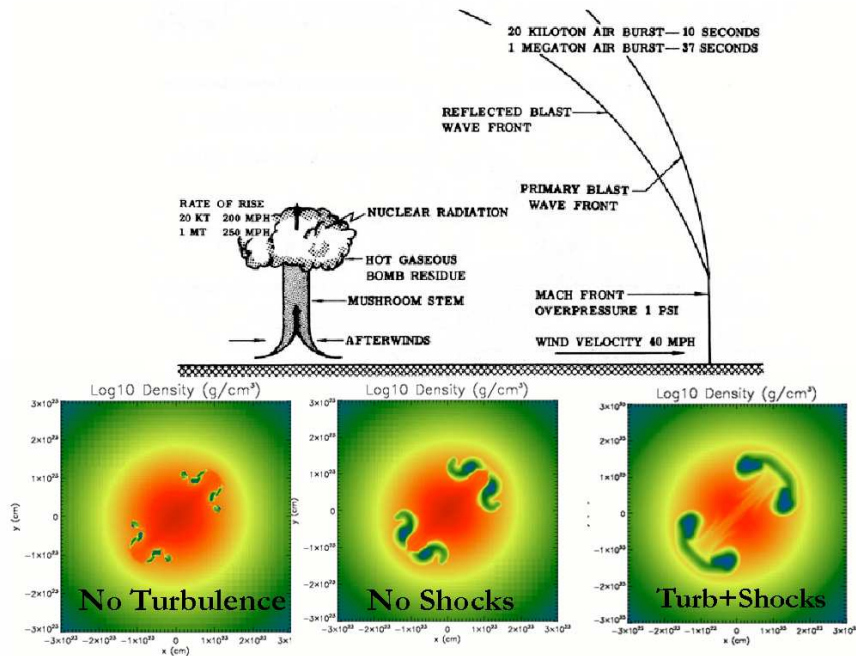


FIGURE 1. Comparison of simulations with and without subgrid model that yields correct results for the Rayleigh-Taylor and Richtmyer-Meshkov instabilities. The panels show slices of the density. The left panel shows a simulation without a subgrid model for turbulence. The right panel shows the effect of supersonic bubble inflation (with a subgrid model).

In a recent paper, Scannapieco & Brüggén (2008) [8] showed that although pure-hydro simulations indicate that AGN bubbles are disrupted into pockets of underdense gas, more detailed modeling of turbulence indicates that this is a poor approximation to a cascade of structures that continues far below current resolution limits. Using a subgrid turbulence model developed by Dimonte & Tipton (2006), they carried out a series of simulations of AGN heating in a cool-core cluster with the adaptive mesh refinement code, FLASH. These simulations showed that Rayleigh-Taylor instabilities act on subgrid scales to effectively mix the heated AGN bubbles with the ICM, while at the same time preserving them as coherent structures (see Fig. 1). The AGN bubbles are thus transformed into hot clouds of mixed material as they move outwards in the hydrostatic medium, much as large airbursts lead to a distinctive “mushroom cloud” structure as they rise in the hydrostatic atmosphere of Earth. This allows X-ray cavities to remain intact out to large distances from the cluster centre while still coupling to the surrounding medium.

Alternatively, it has been suggested that instead of underdense pockets of ideal gas, the cavities are produced by magnetically dominated jets [9]. In 3D MHD simulations by Nakamura et al. [10, 11] bubbles are inflated by a current-carrying jet that injects magnetic flux into a small volume in the vicinity of the supermassive black hole. The jets are launched by injecting non-force-free poloidal and toroidal magnetic fields, and form large currents which travel along the inner jet axis into the lobes and return on the

outer boundary of the lobes, forming a sheath around the jet axis. Like bubbles of hot, underdense gas, such jets expand subsonically into wide lobes that appear cooler than the surrounding medium. Unlike hot, underdense gas, these magnetically dominated bubbles behave differently as they rise through the cluster atmosphere.

Recently, it was investigated whether one can use the measured sizes of X-ray cavities observed at different locations in their host clusters to discriminate between these two models [12]. Compiling the sizes and radial offsets of 64 cavities in the X-ray halos of clusters and groups, they were able to show a tight correlation between these two quantities, which is substantially different than one would expect from simple analytic estimates in the pure-hydro case. From this comparison, they came to the preliminary conclusion that the data favor the current-dominated magneto-hydrodynamic jet model.

While a useful first step, such analytical prescriptions neglect some important physical effects that are likely to affect the interpretation of the data. Whereas the loss of pressure due to bremsstrahlung radiation is negligible, mass entrainment produced by hydrodynamic instabilities is likely to be important [13]. This will add to the growth of the bubbles produced by the expansion during the ascent in the stratified atmosphere. In fact, there is some circumstantial evidence for mass entrainment in FR I radio sources. Croston et al. (2008) [14] showed that equipartition internal pressures are typically lower than the external pressures acting on the radio lobes, so that additional non-radiating particles must be present. A correlation between the structure of the radio sources and the apparent pressure imbalance can be taken as observational evidence that entrainment may provide this missing pressure. Moreover, drag forces and acceleration by buoyancy distort the bubbles, complicating the interpretation of bubble radii.

METHOD

Code

All simulations were performed with FLASH version 3.0, a multidimensional adaptive mesh refinement hydrodynamics code, which solves the Riemann problem on a Cartesian grid using a directionally-split Piecewise-Parabolic Method (PPM) solver. While the direct simulation of turbulence is extremely challenging, computationally expensive, and dependent on resolution [e.g., 15], its behavior can be approximated to a good degree of accuracy by adopting a subgrid approach. The details of the simulation are given in [16]. The reader is referred to this work for these and other related discussions.

X-ray cavities in the ICM are thought to be inflated by a pair of ambipolar jets from an AGN in the central galaxy that inject energy into small regions at their terminal points, which expand until they reach pressure equilibrium with the surrounding ICM. The result is a pair of underdense, hot bubbles on opposite sides of the cluster centre. In order to produce bubbles, we started the simulation by injecting a total energy of E_{inj} into two small spheres of radius $r_{\text{inj}} = 4.5$ kpc at distances of 13 kpc from the cluster centre.

To allow a direct comparison of simulation output with X-ray data, we made use of a newly-developed pipeline for post-processing of gridded simulation output. The

X-ray-imaging pipeline XIM [see also 17] is a publically-available set of scripts that automate the creation of simulated X-ray data for a range of satellites. It takes as input the density, temperature, and velocity, as well as a large number of parameters and provides simulated X-ray data in the form of spectral-imaging data cubes.

XIM is focused on visualizing X-ray data from thermal plasmas. The scripts allow the choice of a user-supplied spectral model as well as the default thermal APEC plasma emission model [18], which self-consistently calculates the equilibrium ionization balance for a thermal plasma. For a fixed set of abundances and a given temperature, APEC then computes interpolated high resolution model X-ray spectra. Atomic data are taken from the ATOMDB using APED [19] and combined with bremsstrahlung continuum for all species.

Having computed the spectral contribution in each cell, XIM then calculated a raw spectral data cube by projecting the data along one of the three Cartesian coordinate axes. Spectra were emission-measure weighted and Doppler shifted with the user-provided radial velocity, neglecting relativistic effects. A user-supplied tracer grid was used to weigh the data by the thermal plasma content of the cell. The spectral grid was oversampled by a factor of three with respect to the final output energy grid to allow accurate representation of Doppler shifts in the output spectra.

The data was further redshifted according to the user-specified cosmological redshift and the coordinate axes are scaled to the proper angular size, given the redshift and cosmological parameters. The flux in a cube (x,y,wavelength) was then scaled to the cosmologically correct flux at the given distance. The projected data were processed for foreground photo-electric absorption using the Wisconsin Absorption Model [WABS 20].

Next, the raw spectral-imaging cube (x,y,wavelength) was re-gridded in the two spatial directions onto the detector plate scale of the user-specified instrument. XIM incorporates telescope parameters for CHANDRA, CONSTELLATION-X, XEUS, and XMM-NEWTON and will incorporate a telescope model for IXO once response matrices become available, in our case the Advanced Imaging Spectrometer (ACIS), on board the CHANDRA X-ray observatory. The re-gridded data cube was then convolved with the appropriate spectral response and ancillary response matrices, and the convolution output was re-gridded onto the user-specified energy grid.

The output was convolved with a model point-spread function for the selected telescope. The current version of XIM is limited to a Gaussian point spread function with energy-independent kernel width. It takes into account quantum efficiency and telescope effective area, but neglects detector non-uniformity, vignetting, and point-spread function variance. Finally, Poisson-distributed photon counts were calculated for a user-specified exposure time.

RESULTS

The differences produced by the subgrid turbulence are significant, especially at times ≥ 150 Myrs. Without the subgrid model, the bubble does not form a single coherent structure but rather looks patchy, eventually coming apart into resolution-dependent subclumps as described in Scannapieco & Brüggén (2008). The cavities in the run

without subgrid turbulence also show a weaker X-ray surface brightness contrast, even though the ambient material gets mixed into the bubble by subgrid turbulence. Current observations of X-ray cavities support this picture, and further observations of bubbles at larger distances from cluster centres will help to probe the stability of the bubbles and check the predictions from these kinds of simulations.

The turbulence also affects the inferred bubble sizes, which have been determined by subtracting a smooth, radially-symmetric background model from the X-ray maps, as is often done with real observations. The corresponding radii are shown in Fig. 2.

We find that analytic estimates as given by Diehl et al. (2008) [12] are not able to capture effects such as mass-entrainment and distortion of the bubbles by drag forces, which are naturally included in the simulation. In fact, our simulations show clearly that the cavities evolve aspherically as they rise through the cluster, expanding quickly in the perpendicular direction, but expanding slowly, or even becoming compressed, in the radial direction.

In our hydrodynamic model of the cavity evolution, the effects of projection are not trivial, and the data points are not just systematically shifted toward smaller radii. The slopes of the size-distance relationship of the bubbles become significantly shallower as the AGN axis tilts toward the line of sight. The appearance of the bubbles show stark differences, especially when the bubbles are further than two bubble radii from the centre of the cluster. Fig. 2 suggest that most observed bubbles come from systems where the AGN axis lies between 90 and 45 degrees from the line of sight. In fact, this is expected geometrically for a random distribution of bubble axes.

In the case where the AGN axis lies at 45 degrees from the line of sight, the bubbles look more like horseshoes. A confirmation of this will require looking for bubbles at greater distances from the centres in clusters where it is believed that the jet axis is inclined not too far from the line of sight. This could help to verify whether the bubbles are mainly hydrodynamic bubbles. One may speculate that the giant cavities found in Abell 2204 resemble these late-stage horse-shoe shaped bubbles [21].

Finally, the pV energy inferred from the observations appears to increase with increasing distance of the bubbles from the cluster centre. This may in part be due to the fact that bubbles tend to be overpressured close to their origin, and expand to reach pressure equilibrium as the rise through the ICM. However, excess pressure in the observed cavities is difficult to measure, except indirectly through the presence of shocks and sound waves.

A second possibility for the radial increase in inferred pV is the entrainment of ambient material. In fact, this is the main reason for the increase in our simulations, as in our model the bubbles quickly reach pressure equilibrium with the surrounding medium, well before moving noticeably out from the cluster centre. Over the 200 Myrs that we simulate, we find that the inferred pV energy for the same bubble grows by a factor of 3-5. The measured energies are more reliable when the bubble are farther from the centre of the cluster, which, unfortunately, is where they are most difficult to observe. Overall, the error introduced into estimates of the pV energy by these effects is of the same magnitude as the error related to the unknown equation of state of the plasma inside the bubbles.

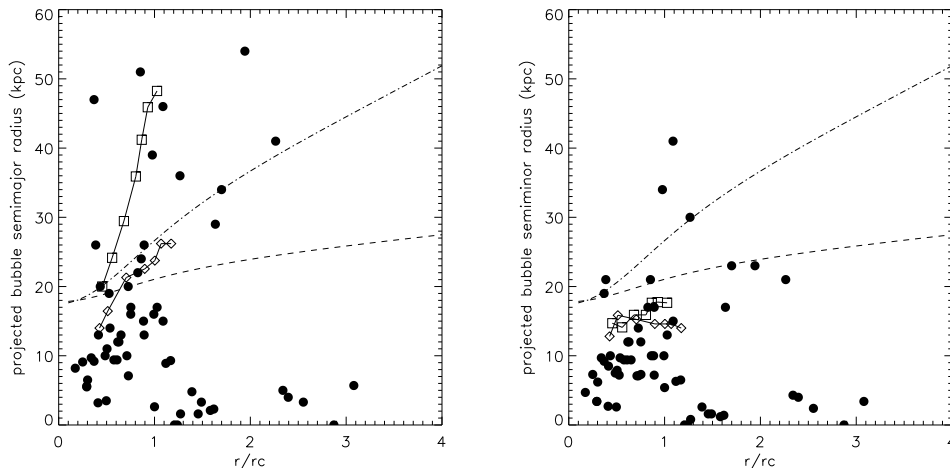


FIGURE 2. Plot of cavity projected radii versus their projected distance from the cluster centres. The connected squares correspond to the measured radii from synthetic observations where the axis of the AGN lies in the plane of the sky. The diamonds correspond to the case where the AGN axis is inclined by 45 degrees with respect to the line of sight. The unconnected filled circles give the sizes of observed cavities compiled in Rafferty et al. (2006). The dashed line shows the prediction for a spherical, adiabatically expanding bubble for $\Gamma = 5/3$, and the dot-dashed line shows the prediction for a current-dominated jet. **Left:** semimajor radii, **Right:** semiminor radii.

CONCLUSIONS

In this study we have focused on a model in which X-ray cavities evolve purely hydrodynamically, and reconstructed their detailed evolution using of two major tools: AMR simulations that include subgrid turbulence and synthetic X-ray software that produces realistic observations from these simulations. Together these tools allow us to capture such important effects as mass-entrainment, distortion of the bubbles by drag forces, and observational effects. These effects lead to an evolution that is drastically different than expected from simple analytic estimates.

In particular, we find that while the radial extent of the cavities changes slowly as a function of distance and time, they expand rapidly in the perpendicular direction. The result is a complex evolution that is highly dependent on viewing angle and difficult to compare conclusively with observations. Although analytic estimates of non-magnetic models evolve too slowly to match the observations, our simulations show that the evolution of the semimajor and semiminor radii is not in obvious contradiction to the data. In fact, our simulations naturally reproduce the overall trend for inferred pV energies of observed X-ray cavities to increase as a function of distance from the cluster centre, an effect that is largely due to mixing of entrained material into the rising cavities. The size evolution we find is in good agreement with the measured bubble sizes, although there is a large spread in observational data, and a strong dependence on the direction from which the cavities are viewed. Indeed, the flattening and projection of X-ray cavities have much stronger effects on our results than initial bubble size and radius.

ACKNOWLEDGMENTS

MB acknowledges the support by the DFG grant BR 2026/3 within the Priority Programme “Witnesses of Cosmic History” and the supercomputing grants NIC 2195 and 2256 at the John-Neumann Institut at the Forschungszentrum Jülich. All simulations were conducted on the Saguaro cluster operated by the Fulton School of Engineering at Arizona State University. The results presented were produced using the FLASH code, a product of the DOE ASC/Alliances-funded Center for Astrophysical Thermonuclear Flashes at the University of Chicago.

REFERENCES

1. P. E. J. Nulsen, D. C. Hambrick, B. R. McNamara, D. Rafferty, L. Birzan, M. W. Wise, and L. P. David, *ApJ* **625**, L9–L12 (2005), [arXiv:astro-ph/0504350](#).
2. M. Brüggen, M. Ruszkowski, and E. Hallman, *ApJ* **630**, 740–749 (2005), [arXiv:astro-ph/0501175](#).
3. S. Heinz, M. Brüggen, A. Young, and E. Levesque, *MNRAS* **373**, L65–L69 (2006), [arXiv:astro-ph/0606664](#).
4. F. Pizzolato, and N. Soker, *MNRAS* **371**, 1835–1848 (2006), [arXiv:astro-ph/0605534](#).
5. K. Robinson, L. J. Dursi, P. M. Ricker, R. Rosner, A. C. Calder, M. Zingale, J. W. Truran, T. Linde, A. Caceres, B. Fryxell, K. Olson, K. Riley, A. Siegel, and N. Vladimirova, *ApJ* **601**, 621–643 (2004), [arXiv:astro-ph/0310517](#).
6. T. W. Jones, and D. S. De Young, *ApJ* **624**, 586–605 (2005), [astro-ph/0502146](#).
7. M. Ruszkowski, T. A. Enßlin, M. Brüggen, S. Heinz, and C. Pfrommer, *MNRAS* **378**, 662–672 (2007), [arXiv:astro-ph/0703801](#).
8. E. Scannapieco, and M. Brüggen, *ApJ* **686**, 927–947 (2008), [0806.3268](#).
9. H. Li, G. Lapenta, J. M. Finn, S. Li, and S. A. Colgate, *ApJ* **643**, 92–100 (2006), [arXiv:astro-ph/0604469](#).
10. M. Nakamura, H. Li, and S. Li, *ApJ* **652**, 1059–1067 (2006), [arXiv:astro-ph/0608326](#).
11. M. Nakamura, H. Li, and S. Li, *ApJ* **656**, 721–732 (2007), [arXiv:astro-ph/0609007](#).
12. S. Diehl, H. Li, C. L. Fryer, and D. Rafferty, *ApJ* **687**, 173–192 (2008), [0801.1825](#).
13. G. Pavlovski, C. R. Kaiser, and E. C. D. Pope, *ArXiv e-prints* (2007), [0709.1796](#).
14. J. H. Croston, M. J. Hardcastle, M. Birkinshaw, D. M. Worrall, and R. A. Laing, *MNRAS* **386**, 1709–1728 (2008), [0802.4297](#).
15. J. Glimm, J. W. Grove, X. L. Li, W. Oh, and D. H. Sharp, *J. Comput. Phys.* **169**, 652–677 (2001), ISSN 0021-9991.
16. M. Brüggen, E. Scannapieco, and S. Heinz, *MNRAS* **395**, 2210–2220 (2009), [0902.4242](#).
17. S. Heinz, and M. Brüggen, *ApJ Submitted* (2009).
18. R. K. Smith, N. S. Brickhouse, D. A. Liedahl, and J. C. Raymond, *ApJ* **556**, L91–L95 (2001), [arXiv:astro-ph/0106478](#).
19. R. K. Smith, N. S. Brickhouse, D. A. Liedahl, and J. C. Raymond, “Standard Formats for Atomic Data: the APED,” in *Spectroscopic Challenges of Photoionized Plasmas*, edited by G. Ferland, and D. W. Savin, 2001, vol. 247 of *Astronomical Society of the Pacific Conference Series*, pp. 161–+.
20. R. Morrison, and D. McCammon, *ApJ* **270**, 119–122 (1983).
21. J. S. Sanders, A. C. Fabian, and G. B. Taylor, *ArXiv e-prints* (2008), [0811.0743](#).